Nanoscale Res Lett (2009) 4:247–253
DOI 10.1007/s11671-008-9233-2

NANO EXPRESS

Synthesis and Characterization of ZnO Nanorods and Nanodisks from Zinc Chloride Aqueous Solution

Tengfa Long · Shu Yin · Kouta Takabatake · Peilin Zhnag · Tsugio Sato

Received: 12 November 2008 / Accepted: 2 December 2008 / Published online: 16 December 2008

Abstract ZnO nanorods and nanodisks were synthesized by solution process using zinc chloride as starting material. The morphology of ZnO crystal changed greatly depending on the concentrations of Zn^{2+} ion and ethylene glycohol (EG) additive in the solution. The effect of thermal treatment on the morphology was investigated. Photocatalytic activities of plate-like $Zn_5(OH)_8Cl_2 \cdot H_2O$ and rod-like ZnO were characterized. About 18% of 1 ppm NO could be continuously removed by ZnO particles under UV light irradiation.

Keywords ZnO nanorod · ZnO nanodisk · Photocatalytic activity · Zinc chloride

Introduction

Zinc oxide with a hexagonal wurtzite crystal structure possesses unique optical and electronic properties, and wide applications on piezoelectric devices, transistors, photodiodes, photocatalysis [1–4], etc. In recent years, much attention has been paid to nanostructure ZnO materials, and various morphologies of ZnO such as nanowire, nanorod, nanotube, nanobelt, nanoring, nanoneedles, and hollow structures, etc. have been developed [5–14]. Many methods have been employed for the morphological control of ZnO crystal, such as pulsed laser deposition(PLD) [15], chemical vapor deposition [16], spray pyrolysis [17, 18], thermal evaporation [19], wet-chemical route [20, 21], etc., in which the wet chemical route has been becoming a charming method due to the mild reaction condition and simplicity of the synthesis process. It is important to prepare well-crystallized and orientated ZnO nanoparticles. In most solution processes for the synthesis of ZnO nanoparticles, zinc acetate, and zinc nitrate are used as starting materials [21–24], but using zinc chloride as a starting material was seldom reported. In the present study, ZnO with rod-like and plate-like structure were successfully synthesized from zinc chloride aqueous solution, and their photocatalytic properties were characterized.

Experimental

$ZnCl_2$, hexamethylenetetramine (HMT, $C_6H_{12}N_4$), ethylene glycol (EG), commercial ZnO powder, butyl acetate, ethyl acetate, and nitrocellulose were used as starting materials. All these chemicals were used as delivered without further purification. Firstly, the cleaned borosilicate glass substrate was coated with thin film of ZnO nanoparticles by a spin-coater (Mikasa 1H-D7). The coating liquid was prepared by uniformly mixing 1 g commercial ZnO nano particles (Sumitomo Osaka Cement ZnO-350) with 2 g of industrial grade nitrocellulose, 5 g of ethyl acetate and 5 g of butyl acetate together with 50 g zirconia balls of 2.7 mm diameter with ball milling using a plastic bottle for 40 h. Then, the prepared substrate was calcined at 400 °C for 1 h. For the second step, the equimolar of $ZnCl_2$ and HMT were dissolved in water or 50 vol.% EG aqueous solution. The ZnO nanoparticles coated glass substrates obtained in the first step were dipped into 50 mL of as-prepared solution containing a desired concentration of $ZnCl_2$–HMT mixture and the

T. Long
Guangxi Normal University, Guilin, People's Republic of China

T. Long · S. Yin (✉) · K. Takabatake · P. Zhnag · T. Sato
IMRAM, Tohoku University, Sendai, Japan
e-mail: shuyin@tagen.tohoku.ac.jp

solution was kept at 95 °C for 12 h in a sealed silicate-glass bottle. Finally, the glass substrate was taken out and washed with distilled water and acetone, then vacuum dried at 80 °C for 1 h. The morphology of the crystals was observed by SEM (Hitachi S-4800) and TEM (JOEL JEM-2000EX). The crystalline phase of the products was determined by X-ray diffraction analysis (XD-01,SHIMADZU). The specific surface area (SSA) was evaluated by nitrogen adsorption–desorption isothermal measurement at 77 K (NOVA-4200e). FT–IR measurements were conducted using the FTS7000 series (DIGILIB). Thermal gravimetry and differential thermal analysis (TG–DTA) curves were traced on a Rigaku Thermoflex (TG8101D) at a heating rate of 10 °C/min in air. The diffuse reflectance spectra of the samples were measured using an UV–vis spectrophotometer (Shimadzu UV-2450). The photocatalytic activity was evaluated by the oxidative destruction of nitrogen monoxide under irradiation of high pressure mercury arc of various light wavelengths using a flow type reactor with a NO_x analyzer (Yanaco, ECL-88A) [25].

Results and Discussion

Figure 1 shows the morphologies of the samples prepared in aqueous solutions of equimolar of $ZnCl_2$–HMT mixture with and without 50 vol.% EG additive. The initial concentrations of Zn^{2+} were 0.01 M, 0.05 M, and 0.1 M, respectively. The morphology of the product changed greatly depending on EG additive and concentration of Zn^{2+}. In the absence of EG, at such low initial $ZnCl_2$–HMT concentration of 0.01 M, the product exhibited uniform spindle-like structure with the length of more than 20 μm (Fig. 1a). When $ZnCl_2$–HMT concentration increased to 0.05 M, hexagonal plate-like morphology with diameter of about 50 μm was formed (Fig. 1b, c). In contrast, with 50 vol.% EG additive in the 0.01 M $ZnCl_2$–HMT mixed aqueous solution, instead of spindle-like structure, ellipse-like head rod structure with smaller size (half length to that of spindle-like structure (Fig. 1a) was formed (Fig. 1d). When the initial concentration of $ZnCl_2$–HMT reached 0.05 M, the morphology changed to a rod-like hexagonal structure (Fig. 1e). When $ZnCl_2$–HMT concentration was 0.1 M, as shown in Fig. 1f, the product exhibited similar hexagonal plate-like morphology to that in the absence of EG, whereas the plate-like particle size decreased to about half to that prepared at the same zinc concentration in the absence of EG (Fig. 1c). These results indicated that zinc ion concentration and EG additive acted very important roles in the morphological control of particles during the solution synthesis process. The existence of EG made the crystals to grow homogeneously due to its good dispersibility and glutinosity. It was also found that in the absence of HMT in 0.1 M $ZnCl_2$ solution, only small amount of products with nonhomogeneous morphologies consisted of spherical and rod-like structure could be obtained, although the image was not shown here.

Figure 2 shows the XRD patterns of the samples prepared in various concentrations of $ZnCl_2$–HMT aqueous solutions with and without 50 vol.% EG additive. The spindle-like particles prepared in 0.01 M $ZnCl_2$–HMT aqueous solution and ellipse-like head rod-like particles and rod-like particles prepared in 0.01 and 0.05 M $ZnCl_2$–HMT–50vol.% EG aqueous solution possessed typical hexagonal wurtzite-type ZnO structure (ICSD No. 89-1397). The relative intensity of (100) and (101) peaks increased with increment of zinc ion concentration. On the other hand, the samples with hexagonal plate-like morphology prepared in 0.05 and 0.1 M $ZnCl_2$–HMT aqueous solution and in 0.1 M $ZnCl_2$–HMT–50% EG aqueous solution displayed quite different diffraction profiles consisting of the peaks at $2\theta = 11.2^{\circ}$, 22.5°, 33.5°, 44.3°, 53.8°

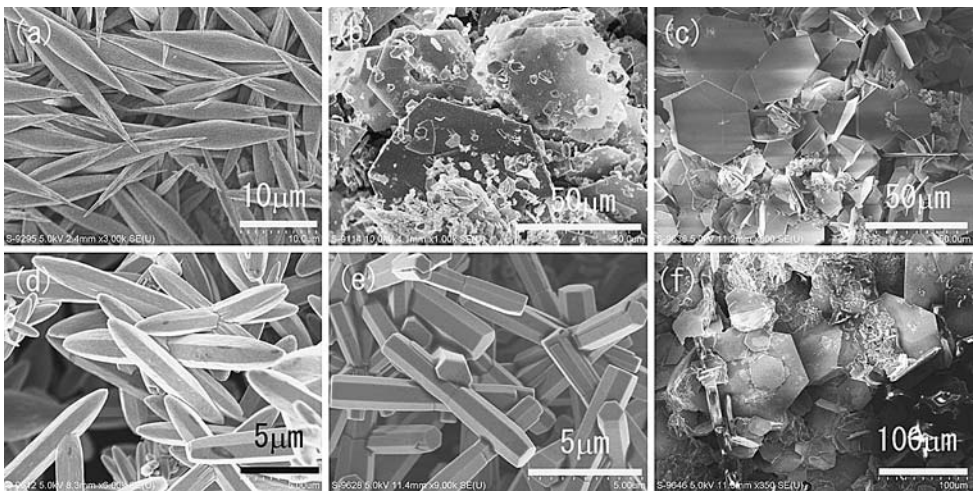

Fig. 1 SEM photographs of the crystals prepared at 95 °C for 12 h in **a** 0.01 M, **b** 0.05 M, **c** 0.1 M $ZnCl_2$–HMT mixed aqueous solution and in **d** 0.01 M, **e** 0.05 M, **f** 0.1 M $ZnCl_2$–HMT mixed 50 vol.% EG aqueous solution

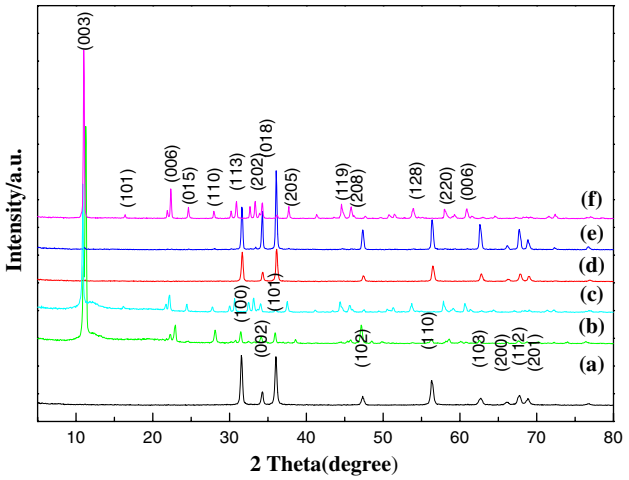

Fig. 2 XRD patterns of the products prepared at 95 °C for 12 h in **a** 0.01 M, **b** 0.05 M, **c** 0.1 M $ZnCl_2$–HMT mixed aqueous solution and in **d** 0.01 M, **e** 0.05 M, **f** 0.1 M $ZnCl_2$–HMT mixed 50 vol.% EG solution. **b**, **c**, **f**: simonkolleite: $Zn_5(OH)_8Cl_2 \cdot H_2O$; **a**, **d**, **e**: wurtzite ZnO

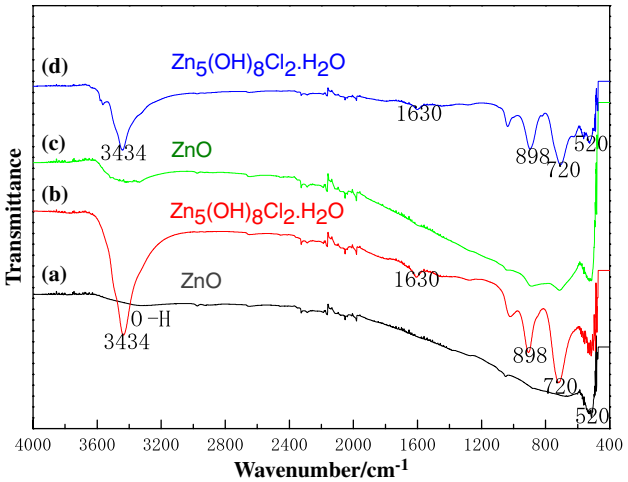

Fig. 3 FT–IR spectra of samples prepared at 95 °C in **a** 0.01 M, **b** 0.05 M $ZnCl_2$–HMT mixed aqueous solution; and those prepared in **c** 0.05 M, **d** 0.1 M $ZnCl_2$–HMT mixed 50 vol.% EG aqueous solution

and 58.3°, which might be ascribed to simonkolleite structure $Zn_5(OH)_8Cl_2 \cdot H_2O$ (ICSD No. 77-2311). These phenomena were quite different with previous results, in which only wurtzite-type ZnO crystals formed using $Zn(NO_3)_2$ and $Zn(CH_3COO)_2$ as Zn^{2+} source. The plate-like structure strongly related to the formation of simonkolleite possessing layered structure [26]. It might be inferred that the high concentration of zinc ion and chloride ion preferred to form simonkolleite structure. Since the formations of ZnO and $Zn_5(OH)_8Cl_2 \cdot H_2O$ shown by Eqs. 1–3, might proceed competitively in the solution, the formation of $Zn_5(OH)_8Cl_2 \cdot H_2O$ became dominant at high chloride ion concentration.

$$HMT \rightarrow Zn(OH)_2 \rightarrow ZnO + H_2O \quad (1)$$

$$Zn^{2+} + 2OH^- \rightarrow Zn(OH)_2 \rightarrow ZnO + H_2O \quad (2)$$

$$5Zn^{2+} + 8OH^- + 2Cl^- + H_2O \rightarrow Zn_5(OH)_8Cl_2 \cdot H_2O \quad (3)$$

The samples with various morphologies prepared in aqueous solution and 50% EG aqueous solution were characterized. Figure 3 shows the FT–IR spectra of the prepared rod-like ZnO and plate-like $Zn_5(OH)_8Cl_2 \cdot H_2O$ samples. It is accepted that zincite (ZnO) only has the bands in the 350–600 cm^{-1} region corresponds to the zinc–oxygen bond [27]. It was obvious that Fig. 3a , c showed the similar spectra with that of ZnO crystal. On the other hand, the samples b and d in Fig. 3 showed quite different spectra to those of Fig. 3a, c. A strong band due to deformation vibration of H_2O molecules at 1,630 cm^{-1}, an absorption band centered at 3,434 cm^{-1} represented the characteristic of an O–H stretching vibration, and intensive bands at 898 and 720 cm^{-1} due to stretching vibration modes of chloride ion [28–30] were observed. These results indicated that simonkolleite ($Zn_5(OH)_8Cl_2 \cdot H_2O$) preferred to be formed at increased chloride ion concentration. These FT–IR data agreed with the XRD patterns shown in Fig. 2.

Figure 4 showed the TG–DTA curves of the hexagonal plate-like simonkolleite samples. The samples prepared in different zinc ion concentration showed similar TG–DTA curves. The weight loss until 100–120 °C was related to the adsorbed water molecules on the surface of the samples. Other two obvious weight loss accompanying with endothermic peak could be observed around 200 and 380 °C, respectively. These weight loss might be ascribed to the dehydration from OH^- groups and release of hydrogen chloride from the simonkolleite $Zn_5(OH)_8Cl_2 \cdot H_2O$ as shown by Eq. 4. [23]

$$Zn_5(OH)_8Cl_2 \cdot H_2O \rightarrow 5ZnO + 4H_2O + 2HCl \quad (4)$$

At high temperature, $Zn_5(OH)_8Cl_2 \cdot H_2O$ decomposed completely to form ZnO. According to Eq. 4, the transformation of simonkolleite $Zn_5(OH)_8Cl_2 \cdot H_2O$ to ZnO results in the weight loss of 26.3 wt%. The weight losses above 120 °C shown in Fig. 4 were 26–28 wt% which agreed well to the calculated value.

To confirm the morphological change and phase transformation behavior of the hexagonal plate-like simonkolleite, the sample was heat treated in air at 300, 600, and 1200 °C, and their XRD patterns and SEM photographs are shown in Figs. 5 and 6, respectively. As shown in Fig. 5, diffraction peaks of simonkolleite gradually disappeared with increment of treatment temperature. After heat treatment at 600 °C, only the characteristic peak of well crystallized ZnO could be observed. In additional, it

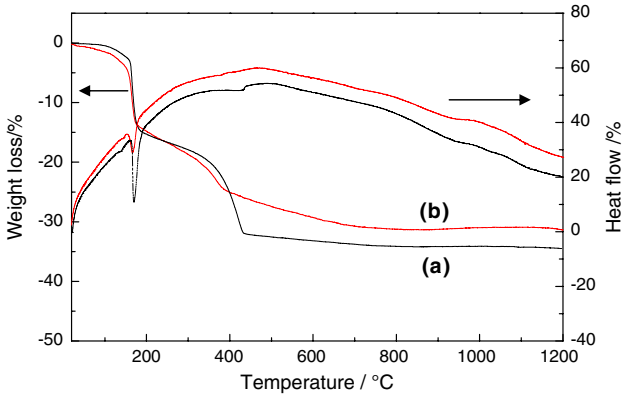

Fig. 4 TG-DTA curves of the typical simonkolleite samples prepared in (**a**) 0.05 M $ZnCl_2$–HMT mixed aqueous solution (**b**) 0.1 M $ZnCl_2$–HMT mixed 50 vol.% EG aqueous solution

might be observed that the (002) peak of the sample prepared by calcination showed higher intensity than those of (100) and (101) peaks, indicating the preferred orientation of ZnO particles, remember usually the ZnO possessed comparatively weak (002) peak intensity (ICSD No. 89-1397).

Figure 6 indicated that the morphology also changed during the heat treatment process. After heat treatment at 300 °C, some weak trace of porous structure on the surface of the samples could be observed. With the increment of treatment temperature, the porosity on the sample surface increased. This behavior related to the decomposition of simonkolleite structure, i.e., the increment of porosity might be caused by the release of water and hydrogen chloride from $Zn_5(OH)_8Cl_2 \cdot H_2O$ at high temperature. Figure 7 shows the TEM photographs of the plate-like $Zn_5(OH)_8Cl_2 \cdot H_2O$ and those after thermal treatment at

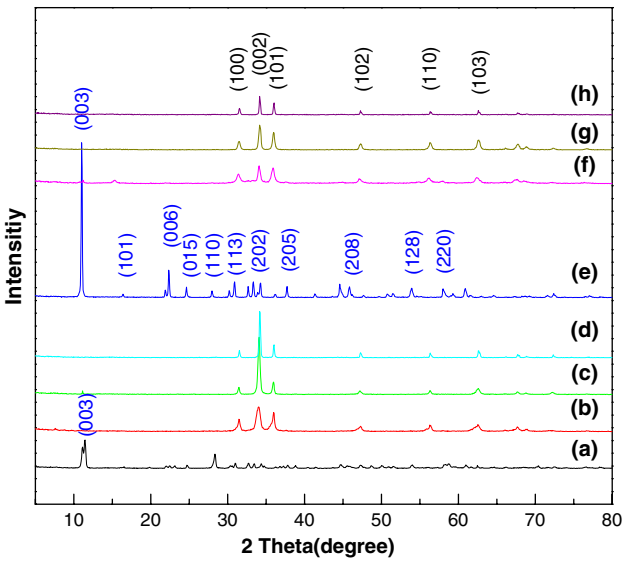

Fig. 5 XRD patterns of samples prepared in (**a**) 0.05 M $ZnCl_2$–HMT mixed aqueous solution followed by calcination at (**b**) 300 °C, (**c**) 600 °C, (**d**) 1200 °C; and in (**e**) 0.5 M $ZnCl_2$ - HMT mixed 50 vol.% EG aqueous solution followed by calcination at (**f**) 300 °C, (**g**) 600 °C, (**h**) 1200 °C

different temperatures. It is obvious that plate-like $Zn_5(OH)_8Cl_2 \cdot H_2O$ possessed smooth surface and those after thermal treatment possessed porous structure, and the porosity increased with treatment temperature.

The SSA and deNO_x photocatalytic activities of the as-prepared samples with different morphologies were characterized. For comparison, a standard titania photocatalyst aeroxide® P25 was also characterized and the results are summarized in Table 1. The aeroxide®\P25 titania powder is usually used as a reference sample in photocatalytic

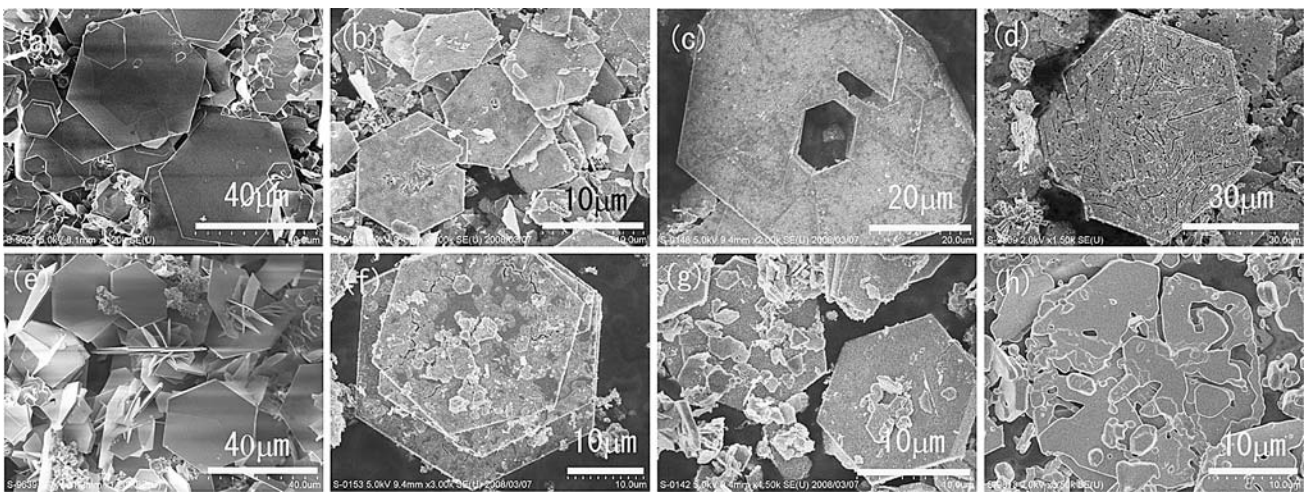

Fig. 6 SEM images of samples prepared in (**a**) 0.05 M $ZnCl_2$–HMT mixed aqueous solution followed by calcination at (**b**) 300 °C, (**c**) 600 °C, (**d**) 1200 °C; and in (**e**) 0.1 M $ZnCl_2$–HMT mixed 50 vol.% EG aqueous solution followed by calcination at (**f**) 300 °C, (**g**) 600 °C, (**h**) 1200 °C

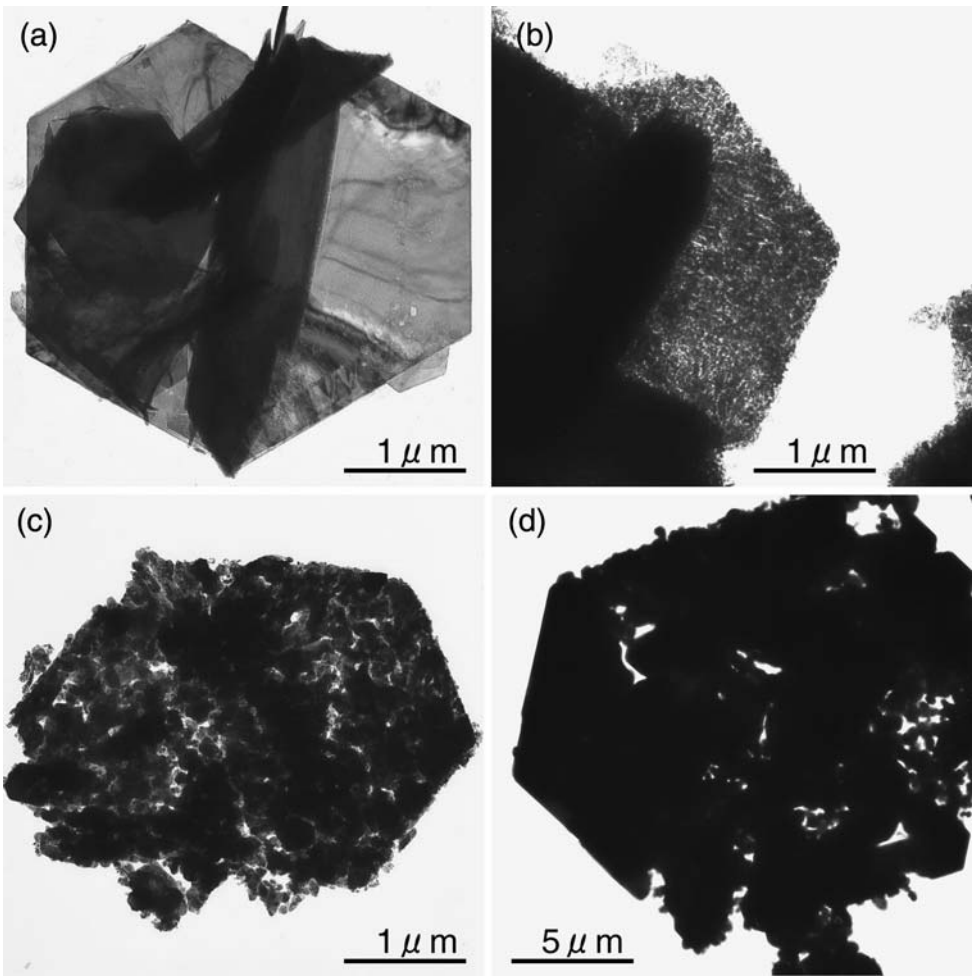

Fig. 7 TEM images of samples prepared in (**a**) 0.1 M $ZnCl_2$–HMT mixed 50 vol.% EG aqueous solution followed by calcination at (**b**) 300 °C, (**c**) 600 °C, (**d**) 1200 °C

Table 1 SSA and deNO_x ability of the samples prepared under different conditions, together with those of P25 titania

Sample	Synthesis condition	Morphology	SSA (m^2/g)	DeNO_x photocatalytic activity (%)	
				>410 nm	>290 nm
P25 Titania AEROXIDE®	Commercial	–	55.9	28.3	37.5
ZnO	0.01 M $ZnCl_2$–HMT mixed aqueous solution	Spindle-like	4.3	4.25	18.1
$Zn_5(OH)_8Cl_2 \cdot H_2O$	0.05 M $ZnCl_2$–HMT mixed aqueous solution	Plate-like	19.4	2.01	11.7
ZnO	0.05 M $ZnCl_2$–HMT mixed 50% EG solution	Hexagonal rod-like	3.2	0	17.7
$Zn_5(OH)_8Cl_2 \cdot H_2O$	0.1 M $ZnCl_2$–HMT mixed 50% EG solution	Plate-like	19.7	0	11.2

research, because of its high photocatalytic activity. As shown in the Table 1, the $Zn_5(OH)_8Cl_2 \cdot H_2O$ with hexagonal plate-like structure prepared in both water or 50vol.% EG aqueous solution showed such high BET specific surface areas as 19.4 m^2/g and 19.7 m^2/g, respectively, while those of the as-prepared rod-like ZnO showed low values of 3–4 m^2/g, however, ZnO samples showed higher deNO_x activity than those of $Zn_5(OH)_8Cl_2 \cdot H_2O$. The high SSA of the simonkolleite might be related to its very thin plate-like structure. Although the prepared samples showed lower photocatalytic activity compared with commercial titania powders, it was notable that about 18% of 1 ppm NO was continuously removed under UV light irradiation.

Figure 8 shows the DRS spectra of the samples prepared at 95 °C in $ZnCl_2$–HMT mixed aqueous solution and 50 vol.% EG aqueous solution together with that of commercial ZnO. The spindle-like ZnO showed similar DRS

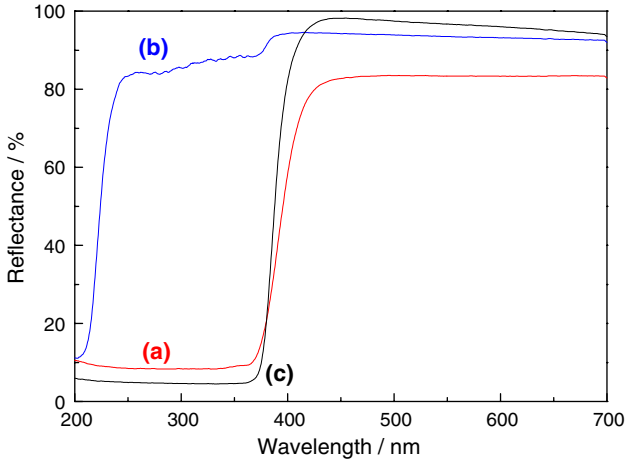

Fig. 8 DRS spectra of samples prepared at 95 °C in (**a**) 0.01 M $ZnCl_2$–HMT mixed aqueous solution (spindle-like ZnO), (**b**) 0.1 M $ZnCl_2$–HMT mixed 50 vol.% EG aqueous solution (plate-like simonkolleite). (**c**) commercial ZnO

spectra with that of commercial ZnO powders, while that of plate-like simonkolleite showed quite different spectra, indicating very low absorption ability of UV light above 290 nm. This result agreed with those in Table 1, in which the ZnO samples showed higher photocatalytic deNO_x ability than those of plate-like simonkolleite samples although the SSA was smaller.

Conclusions

Based on above results, the following conclusions might be drawn: The morphology and crystalline phase of the product by the heat treatment of $ZnCl_2$–HMT aqueous solution with and without EG changed greatly depending on the concentrations of Zn^{2+} ion and EG additive in the solution. Layered hexagonal plate-like $Zn_5(OH)_8Cl_2 \cdot H_2O$ were formed in 0.05 M and 0.1 M $ZnCl_2$–HMT mixed aqueous solution and in 0.1 M $ZnCl_2$–HMT mixed 50 vol.% EG aqueous solution. The existence of EG in the solution promote the homogeneous crystal growth, and also delay the formation of hexagonal plate-like structure. Hexagonal plate-like $Zn_5(OH)_8Cl_2 \cdot H_2O$ have comparatively higher SSA than that of rod-like ZnO crystal fabricated by the same method. Although the prepared ZnO samples showed lower photocatalytic activity compared with commercial titania powders, about 18% of 1 ppm NO was continuously removed.

Acknowledgments This research was carried out as one of the projects under the Special Education and Research Expenses on "Post-Silicon Materials and Devices Research Alliance" and the JSPS Asian Core Program "Interdisciplinary Science of Nanomaterials", JSPS Core University Program (CUP), supported by Nippon Sheet Glass Foundation for Materials Science and Engineering, Research for Promoting Technological Seeds, JST, and a Grant-in-Aid for Science Research (No.20360293).

References

1. Y.W. Zhu, H.Z. Zhang, X.C. Sun, S.Q. Feng, J. Xu, Q. Zhao, B. Xiang, R.M. Wang, Appl. Phys. Lett. **83**, 144–146 (2003). doi:10.1063/1.1589166
2. K. Keis, C. Bauer, G. Boschloo, A. Hagfeldt, K. Westermark, H. Rensmo, H. Siegbahn, J. Photochem. Photobiol. A Chem. **148**, 57–64 (2002)
3. L. Luo, Y. Zhang, S.S. Mao, L. Lin, Sens. Actuators A Phys. **127**, 201–206 (2006). doi:10.1016/j.sna.2005.06.023
4. Y. Zhang, F. Zhu, J. Zhang, L. Xia, Nanoscale Res. Lett. **3**, 201–204 (2008). doi:10.1007/s11671-008-9136-2
5. Z.L. Wang, J. Song, Science **312**, 242–246 (2006). doi:10.1126/science.1124005
6. X.M. Sun, X. Chen, Z.X. Deng, Y.D. Li, Mater. Chem. Phys. **78**, 99–104 (2003). doi:10.1016/S0254-0584(02)00310-3
7. Y.X. Chen, X.Q. Zhao, B. Sha, J.H. Chen, Mater. Lett. **62**, 2369–2371 (2008). doi:10.1016/j.matlet.2007.12.004
8. Z.W. Pan, Z.R. Dai, Z.L. Wang, Science **291**, 1947–1949 (2001). doi:10.1126/science.1058120
9. X.Y. Kong, Y. Ding, R. Ying, Z.L. Wang, Science **303**, 1348–1351 (2004). doi:10.1126/science.1092356
10. T.Y. Kim, J.Y. Kim, S.H. Lee, H.W. Shim, S.H. Lee, E.K. Suh, K.S. Nahm, Synth. Met. **144**, 61–68 (2004). doi:10.1016/j.synthmet.2004.01.010
11. L.M. Shen, N.Z. Bao, K. Yanagisawa, K. Domen, C.A. Grimes, A. Gupta, J. Phys. Chem. C **111**, 7280–7287 (2007). doi:10.1021/jp0708603
12. C. Yan, D. Xue, Funct. Mater. Lett. **1**, 37–42 (2008). doi:10.1142/S1793604708000083
13. C. Yan, D. Xue, J. Phys. Chem. B **110**, 7102–7106 (2006). doi:10.1021/jp057382l
14. C. Yan, J. Liu, J. Wu, K. Gao, D. Xue, Nanoscale Res. Lett. **3**, 473–480 (2008). doi:10.1007/s11671-008-9193-6
15. T.K. Subramanyam, B. Srinivasulu Naidu, S. Uthanna, Cryst. Res. Technol. **35**, 1193–1202 (2000). doi:10.1002/1521-4079(200010)35:10<1193::AID-CRAT1193>3.0.CO;2-6
16. X. Zhang, S.Y. Xie, Z.Y. Jiang, X. Zhnag, Z.Q. Tian, Z.X. Xie, R.B. Huang, L.S. Zheng, J. Phys. Chem. B **107**, 10114–10118 (2003). doi:10.1021/jp034487k
17. J. Wienke, A.S. Booij, Thin Solid Films **516**, 4508–4512 (2008). doi:10.1016/j.tsf.2007.05.078
18. T. Dedova, O. Volobujeva, J. Klauson, A. Mere, M. Krunks, Nanoscale Res. Lett. **2**, 391–396 (2007). doi:10.1007/s11671-007-9072-6
19. A. Umar, S.H. Kim, J.H. Kim, Y.B. Hahn, Mater. Lett. **62**, 167–171 (2008). doi:10.1016/j.matlet.2007.04.098
20. P. Jiang, J.J. Zhou, H.F. Fang, Mater. Lett. **60**, 2516–2521 (2006). doi:10.1016/j.matlet.2006.01.041
21. S. Yin, T. Sato, J. Mater. Chem. **15**, 4584–4587 (2005). doi:10.1039/b512239b
22. S. Yin, R. LI, T. SATO, Adv. Sci. Technol. **45**, 679 (2006)
23. H. Bahadur, A.K. Srivastava, R.K. Sharma, S. Chandra, Nanoscale Res. Lett. **2**, 469–475 (2007). doi:10.1007/s11671-007-9089-x
24. T. Long, K. Takabatake, S. Yin, T. Sato, J. Cryst. Growth, in press (2008). doi: 10.1016/j.jcrysgro.2008.09.048
25. S. Yin, H. Hasegawa, D. Maeda, M. Ishitsuka, T. Sato, J. Photochem. Photobiol. A Chem. **163**, 1–8 (2004). doi:10.1016/S1010-6030(03)00289-2

26. W.X. Zhang, K. Yanagisawa, Chem. Mater. **19**, 2329–2334 (2007). doi:10.1021/cm0626841
27. Q. Qu, C. Yan, Y. Wan, C. Cao, Corros. Sci. **44**, 2789–2803 (2002). doi:10.1016/S0010-938X(02)00076-8
28. N.V. Bhat, M.M. Nate, M.B. Kurup, V.A. Bambole, Nucl. Instrum. Methods Phys. Res. B **262**, 39–45 (2007)
29. T. Ishikawa, K. Matsumoto, K. Kandori, T. Nakayama, Colloids Surf. A Physicochem. Eng. Asp. **293**, 135–145 (2007). doi:10.1016/j.colsurfa.2006.07.018
30. H. Tanaka, A. Fujioka, A. Futoyu, K. Kandori, T. Ishikawa, J. Solid State Chem. **180**, 2061–2066 (2007). doi:10.1016/j.jssc.2007.05.001